Hindawi
Mathematical Problems in Engineering
Volume 2020, Article ID 4065351, 11 pages
https://doi.org/10.1155/2020/4065351

Research Article

Estimation of Continuous Joint Angles of Upper Limb Based on sEMG by Using GA-Elman Neural Network

Junhong Wang[1,2] **Qiqi Hao**[1] **Xugang Xi**[1] **Jiuwen Cao**[1] **Anke Xue**[1] **and Huijiao Wang**[1]

[1]*Artificial Intelligence Institute, Hangzhou Dianzi University, Hangzhou 310018, China*
[2]*Department of Mechanical and Electrical Engineering, Xinjiang Institute of Technology, Akesu 843100, China*

Correspondence should be addressed to Junhong Wang; junhongwang@hdu.edu.cn and Anke Xue; akxue@hdu.edu.cn

Received 14 December 2019; Revised 21 April 2020; Accepted 30 May 2020; Published 13 July 2020

Academic Editor: Carlo Renno

The estimation of continuous and simultaneous multijoint angle based on surface electromyography (sEMG) signal is of considerable significance in rehabilitation practice. However, there are few studies on the continuous joint angle of multiple joints at present. In this paper, the wavelet packet energy entropy (WPEE) of the special subspace was investigated as a feature of the sEMG signal. An Elman neural network optimized by genetic algorithm (GA) was established to estimate the joint angle of shoulder and elbow. First, the accuracy of the method is verified by estimating the angle of the shoulder joint. Then, this method was used to simultaneously and continuously estimate the shoulder and elbow joint angle. Six subjects flexed and extended the upper limbs according to the intended movements of the experiment. The results show that this method can obtain a decent performance with a RMSE of 3.4717 and R^2 of 0.8283 in shoulder movement and with a RMSE of 4.1582 and R^2 of 0.8114 in continuous synchronous movement of the shoulder and elbow.

1. Introduction

Hemiplegia is a motor dysfunction caused by nerve damage [1, 2]. Clinical treatment for hemiplegic patients is mainly treated by one-to-one manual treatment by therapists [3]. This approach is time-consuming and cannot be quantified and objectively evaluated. Therefore, a new and efficient rehabilitation therapy is urgently needed to make up for the shortcomings of traditional rehabilitation training. Robots are used to participate in rehabilitation training, freeing therapists from major physical work, monitoring and evaluating the training process, and developing better rehabilitation programs for patients. The effect of rehabilitation has been greatly improved [4–6].

Surface electromyography (sEMG) signals can reflect neuromuscular activity to a certain extent, and its collection process is convenient and harmless to the human body. It can adapt to the particularity of the physiological condition of hemiplegic patients. Therefore, it becomes one of the most vital signals that can directly reflect the intended movement of the human body. It is used as a tool to indicate the body's paralysis of the arm all the time [7].

Many researchers use forces, torques, and angles estimated from SEMG signals to predict movement, thus driving the upper limb movement of the rehabilitation device [8–11]. In the rehabilitation system, the movement intention of the human body must be continuously recognized from sEMG. Robots can match human intentions to perform effective assistance. Pan et al. [12] extracted the stationary component of sEMG and used the time domain feature set to characterize sEMG. Linear discriminant analysis classifier and state space model are used for action classification and angle estimation. Han et al. [13] integrated forward dynamics into the HMM and used the extended HMM to directly estimate the joint motion state. Zhang et al. [14] used principal component analysis and independent component analysis to decompose sEMG mode, respectively. The artificial neural network was used to continuously estimate four joint angles of shoulder joint and elbow joint at the same time. Huang et al. [15] proposed a Gaussian

mixture model for clustering to achieve the purpose of divide and conquer in the simultaneous control of hand and wrist movements. Xiao et al. [16] proposed a multidelay feature signal of surface EMG and used random forest to improve the estimation of joint angle accuracy. Ding et al. [17] proposed a redundant segmentation method based on association. They established a state space frame of the motion model to estimate the angle of multiple joints. Liu et al. [18] established a nonlinear autoregressive exogenous model based on myoelectric signals to continuously estimate angles of shoulder, elbow, and wrist motions. However, the performance of the motion estimation in these documents is still unsatisfactory. Although the model structure is optimized, the training model process is complicated and the calculation amount is large [13, 17]. In other literature, the model is simple and does not adjust the model structure to improve performance. Therefore, this paper uses the Elman neural network with feedback. Considering that the BP algorithm is easy to fall into local optimization, genetic algorithm (GA) to optimize Elman is used.

There are still some difficulties in synchronous motion intention recognition of shoulder and elbow joints. The movement of the shoulder and elbow is more extensive. And in the extensive movement of the upper limb, there are many changes in the shoulder and elbow. Therefore, it is more meaningful to estimate the degree of freedom of shoulder joint and elbow joint continuously at the same time.

In this study, we studied the feature method of wavelet packet energy entropy for specific subspaces to alleviate the redundancy problem of adjacent subspaces. For proportional control of shoulder and wrist movements, GA-Elman is used to improve prediction accuracy. The sEMG signals and upper limb movements are recorded during various dynamic processes. In the continuous movement of the shoulder, the feature method and proportional control strategy are discussed and verified to improve the prediction accuracy. The reliability of using this method is discussed in shoulder and elbow synchronous continuous motion.

2. Materials and Methods

2.1. Data Acquisition. Six healthy subjects (three males and three females, age 22–28, height 160–180 cm, weight 48–70 kg) were enrolled in this study. They are right-handers. All the subjects read and signed an informed consent form approved by an institutional review board. Before the experiment, everyone was asked to practice as expected to adapt to the equipment until they felt comfortable. In this experiment, Trigno Wireless System (Delsys Inc, Natick, MA, USA) was used to record sEMG signals at a sampling frequency of 1600 Hz. The real angle measurement of shoulder and elbow joints is based on the Codamotion System (Charnwood Dynamics Ltd, UK), which is an active optical motion capture system introduced. The frequency of the acquisition angle is 200 Hz. The average subsampling processing method was used to make the frequency the same. Before collecting sEMG, the muscle surface of volunteers was wiped with alcohol. And the sensors were attached according to the standard manual. We selected eight muscle channels, which in order are biceps brachii, triceps brachii, deltoid (anterior), pectoralis major, deltoid (middle), brachioradialis, trapezius, and teres minor muscle. The sEMG sensors were placed over eight muscles and the markers of Codamotion were set over shoulders and elbows, as shown in Figure 1.

During the experiment, the subject sat quietly in the chair. The subject's right arm hanged naturally and the right hand relaxed. All movements started from where their arm fell naturally and returned to this position after the action was completed. The initial state is shown in Figure 2(a).

The experimental movement is shown in Figure 2. In Figure 2(b), subjects were asked to touch their right shoulders in a direction perpendicular to the human body with their right hand. In Figure 2(c), the subject was required to lift the right arm as much as possible in a direction perpendicular to the human body. In Figure 2(d), the subject was required to lift the right arm as much as possible in the horizontal direction of the human body. After each movement, the right arm returned to the initial position. Each subject's four movements were performed in 10 s in sequence, and each subject performed a total of 120 groups of movements. Each experiment was timed with a stopwatch to ensure that one experiment was completed in about ten seconds. The experiment was completed in six days. Each group completed 20 experiments per day. To ensure that the results were not affected, the experimental environment was the same every day. The subjects rested for 10 s to reduce the effects of muscle fatigue after completing a group movement.

2.2. Data Processing. The raw signal was denoised using a wavelet transform. Wavelet packet transform has good signal decomposition ability. Therefore, a sEMG feature extraction method was studied based on that. Wavelet packet transform decomposes the low-frequency part and the high-frequency part of the subspace at the same time, which has better time-frequency localization analysis ability than the wavelet transform [19].

Six-layer wavelet packet decomposition is performed on eight-channel sEMG signals, and db4 wavelet was chosen as the wavelet base. The raw sEMG signal is very weak, and its energy is mainly distributed in the frequency range of 10–500 Hz [20, 21]. Extracting the signal features in the 25–400 Hz band can filter out the high-frequency noise and unnecessary low-frequency information [22].

There is a different degree of information redundancy between adjacent subspaces [23], due to the proximity of frequency. Therefore, the entropy characteristics of nonadjacent subspace P_i^j (i is the i-th wavelet packet decomposition. j is the j-th subspace of the i-th layer) are selected in this paper. We extracted the wavelet packet energy entropy (WPEE) in the 25–400 Hz (P_6^2: 25–50 Hz, P_5^2: 50–100 Hz, P_4^2: 100–200 Hz, P_3^2: 200–400 Hz) frequency band as Feature A. The wavelet packet energy entropy in the subspace (P_4^1: 0–100 Hz, P_4^2: 100–200 Hz, P_4^3: 200–300 Hz, P_4^4: 300–400 Hz) on the same decomposition layer is taken as Feature B. The subspace of wavelet packet decomposition is shown in Figure 3. The raw signal and the specific frequency band signal after wavelet packet decomposition are shown in

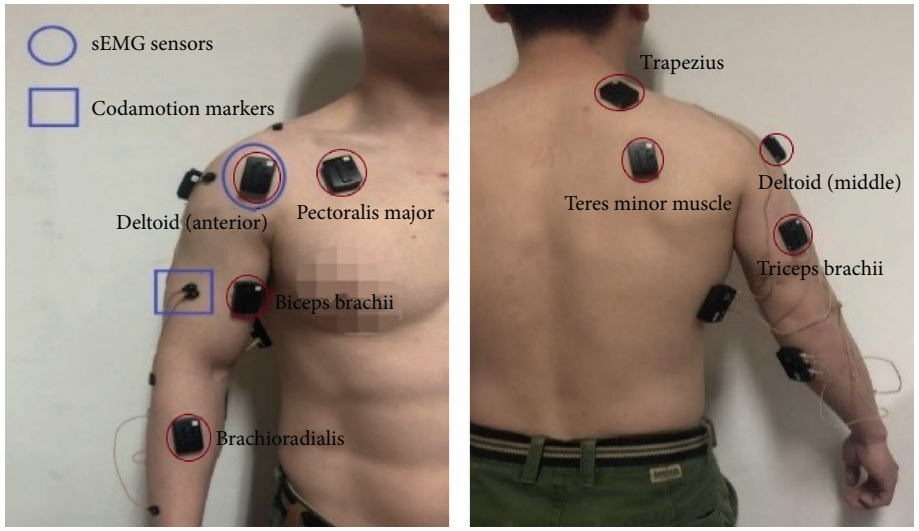

Figure 1: Sensors and markers placement.

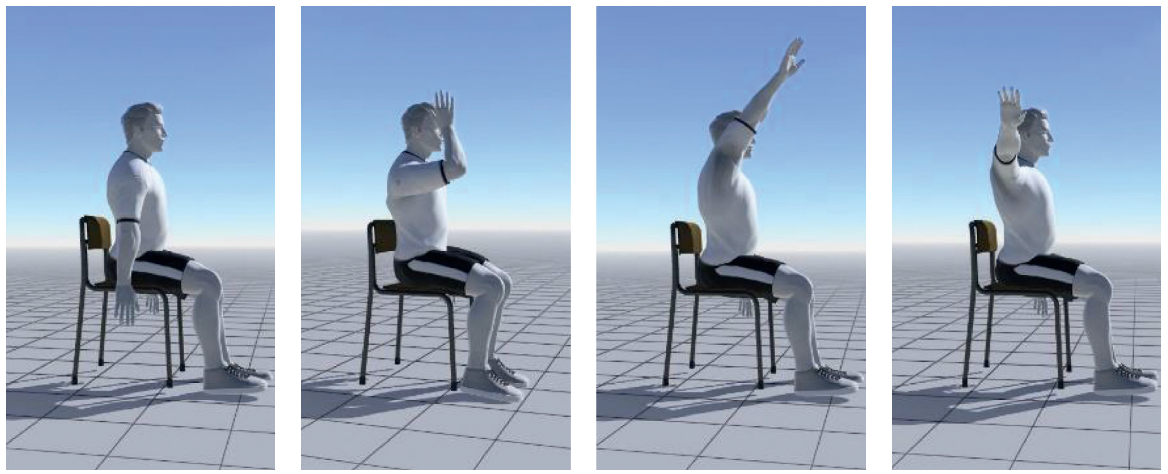

Figure 2: Movement description. (a) The initial state of the subject. The arms are naturally lowered vertically. (b) The subject touched his right shoulder. (c, d) Subjects lifted the right arm as much as possible in different directions.

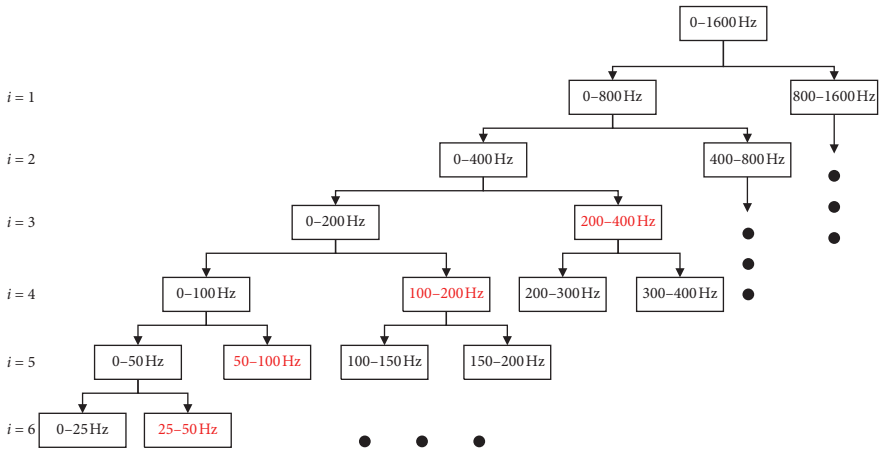

Figure 3: The subspace of wavelet packet decomposition (red is the subspace selected as Feature A; i is the index of the number of decomposition layers).

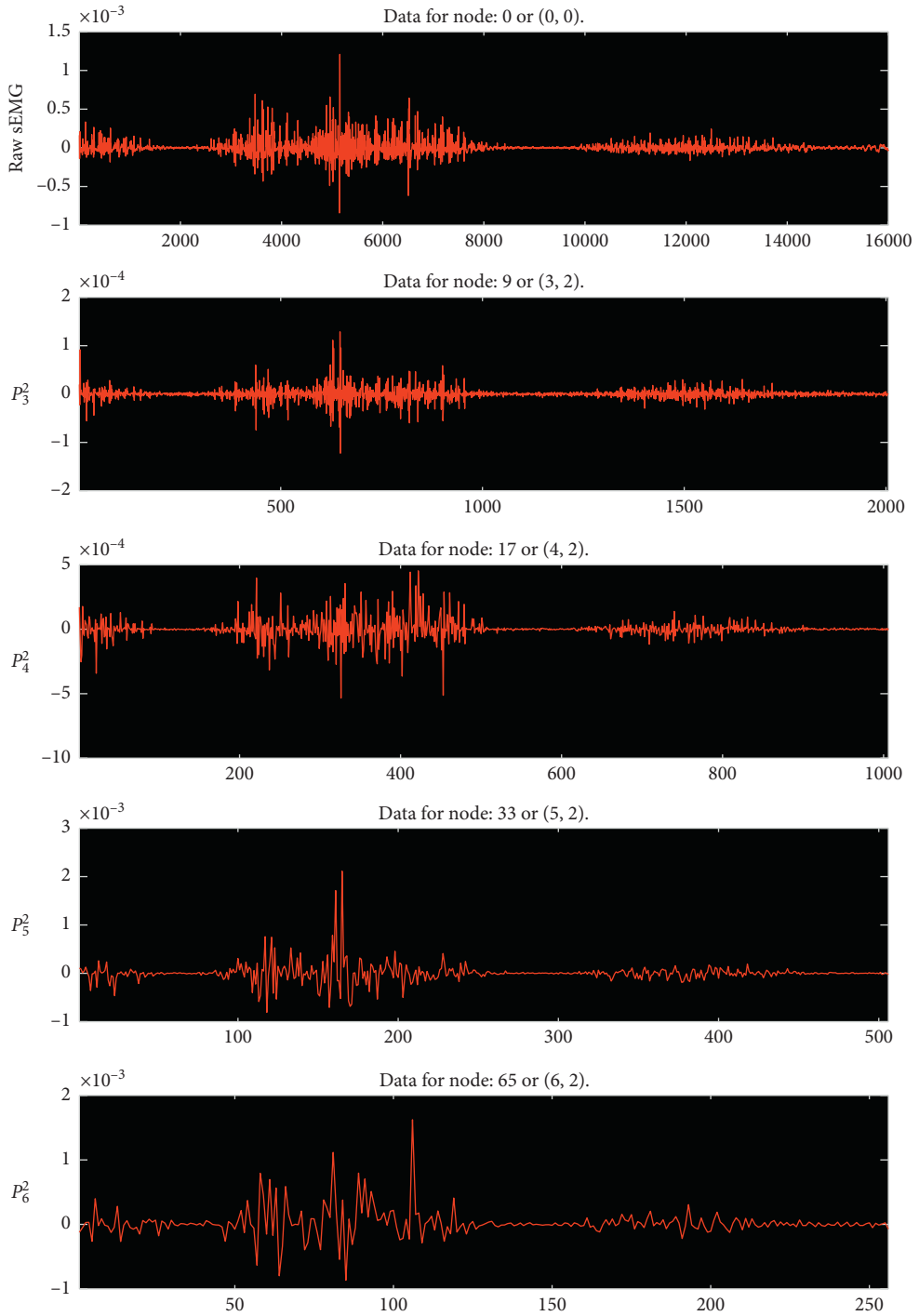

Figure 4: The raw signal and the signal after wavelet packet decomposition.

Figure 4. The raw signal is from brachioradialis muscle which mainly acts on elbow joint movement.

2.3. Optimized Elman Neural Network for Angle Estimation

2.3.1. Structure of Elman Neural Network. The general Elman NN has four layers: the input layer, the implicit layer, the bearing layer, and the output layer. The block diagram of Elman NN is shown in Figure 5. Its input node is 32, hidden node is 20, and output node is 1. The bearing layer of the Elman NN preserves the output of the hidden layer at the previous moment and then adds it to the input of the hidden layer at the next moment [24]. This self-connected mode can make the network have the memory function and sensitivity to the historical data, so it can model dynamically and strengthen the ability of the network to process the dynamic information.

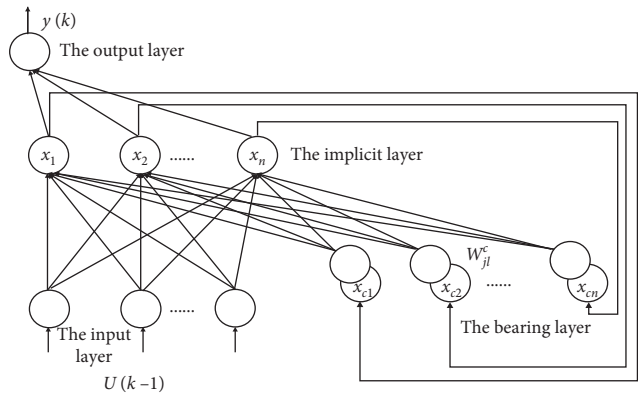

Figure 5: The block diagram of Elman NN.

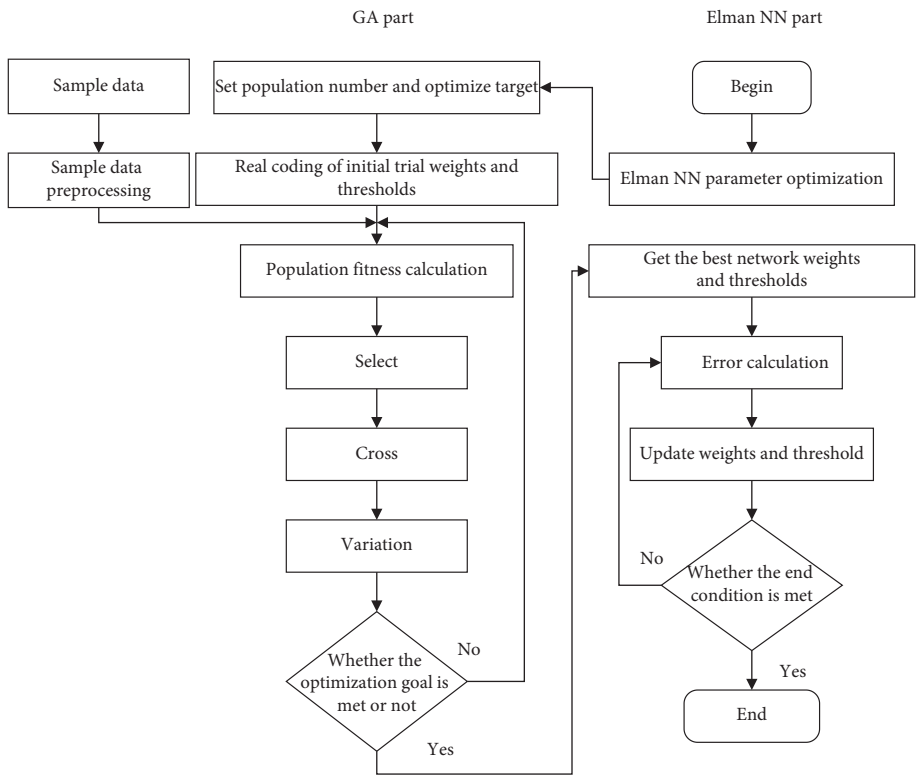

Figure 6: Flowchart of GA-Elman algorithm.

2.3.2. Genetic Algorithm (GA) Theory and GA-Elman. BP algorithm is easy to fall into local minima [25]. Genetic algorithm (GA) can alleviate this problem. The fuzzy roulette wheel selection and a new mutation operator method in genetic algorithm were used to avoid falling into the optimal local problem [26]. The GA is chosen to train the parameters of Elman neural network (GA-Elman NN) model. Starting from any initial population, GA generates a new group of individuals through random selection, crossover, and mutation operations. It has evolved the population into areas that are getting better and better in the search space. In this way, after a generation of genetic optimization, the optimal solution is finally obtained.

The flowchart of optimizing Elman neural network with GA is shown in Figure 6. The sEMG signals need to be preprocessed before network training. In GA-Elman NN, the parameters of the Elman NN are first initialized to determine the initial parameters and optimization goals of the genetic algorithm. Then, the initial weights and thresholds of the Elman NN are genetically encoded, the fitness values of individuals in the population are calculated, and genetic operations such as cross-mutation are selected. Next, it is judged whether the optimal weight and threshold are obtained. If obtained, the Elman NN is trained using optimal weights and thresholds. If not obtained, multiple genetic manipulations are performed until they are obtained.

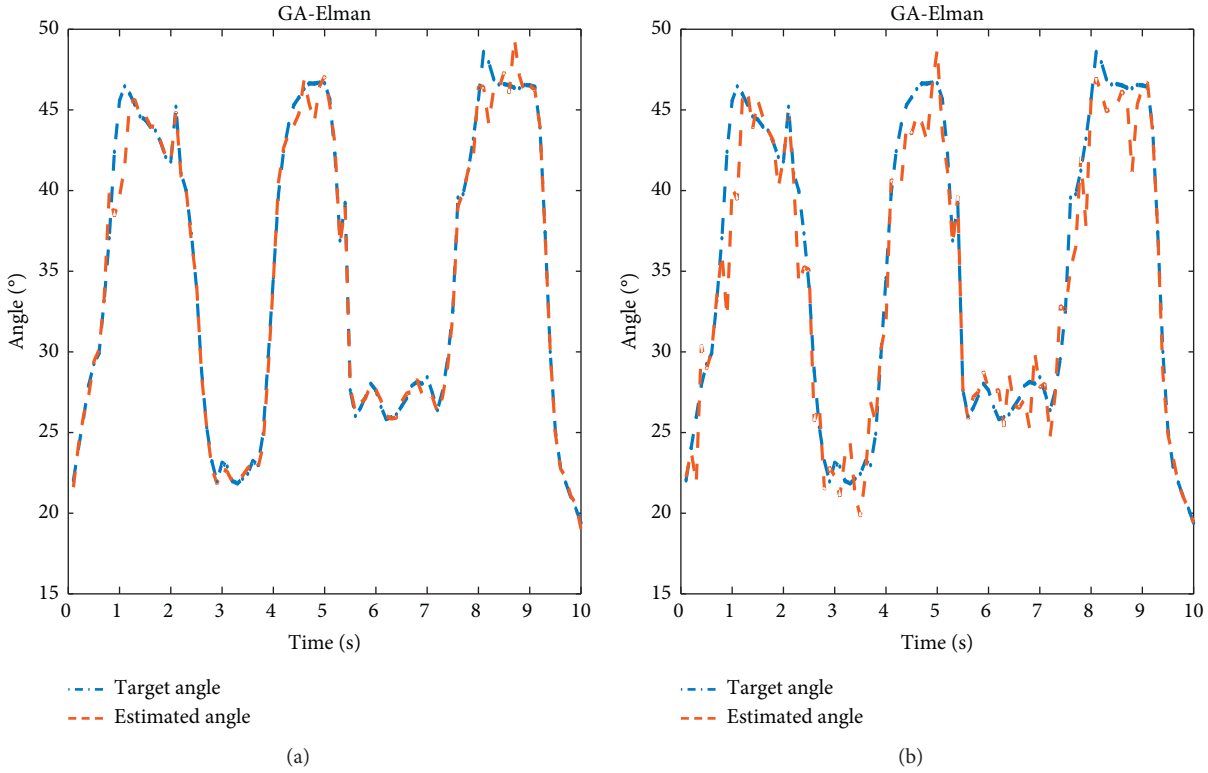

Figure 7: Comparison of the estimated shoulder joint angles and the actual shoulder joint angles by using GA-Elman with (a) Feature A and (b) Feature B.

Elman NN training is performed again. Finally, the Elman NN training gets the training error that satisfies the condition, and the whole method ends. The parameters of GA-Elman are obtained according to a large number of experiments [26].

GA-Elman can be regarded as an adaptive system without manual intervention [27]. It can automatically adjust the connection weight and structure and realize the integration of GA and Elman. According to the relationship between the sEMG and the movement of the shoulder joint and the elbow joint, we use sEMG eigenvector as input of Elman NN, and shoulder joint angle and elbow joint angle were used as the output of the neural network. Through the construction and training network, the mapping relationship between sEMG and the joint angle signal is established.

3. Results and Discussion

All assessments were based on data from 6 healthy subjects. K-fold validation ($k = 6$) is adopted, with 1 out of k repetitions of each movement as the test set and the rest as the training set. In this discussion, the angle estimation results of the shoulder joint are used to verify the accuracy and superiority of the method.

In this paper, average root mean square error (RMSE) and average coefficient of determination (R^2) are used to evaluate the estimation performance. The RMSE is calculated as follows:

$$\text{RMSE} = \sqrt{\frac{\sum_{n=0}^{N} \left(\widehat{y_n} - y_n\right)^2}{N}}, \tag{1}$$

where N is the length of the joint angle, $\widehat{y_n}$ is the predicted joint angle, and y_n is the real joint angle. R^2 is calculated as follows:

$$R^2 = 1 - \frac{\sum_{n=0}^{N} \left(\widehat{y_n} - y_n\right)^2}{\sum_{n=0}^{N} \left(y_n - \overline{y_n}\right)^2}, \tag{2}$$

where y_n is the real joint angle, $\overline{y_n}$ is the mean of y_n, and $\widehat{y_n}$ is the estimated joint angle. R^2 is between 0 and 1. The closer to 1, the better the regression fitting effect. It is generally believed that the model with a fit of more than 0.8 has a higher degree of goodness of fit.

3.1. Estimation of Shoulder Joint Angle. The GA-Elman network of upper limb shoulder movement was established for each subject. The comparison of the estimated shoulder joint angles and the actual shoulder joint angles of one subject by using GA-Elman with Feature A and Feature B is shown in Figure 7.

As can be seen from Figure 7, the fitting result using Feature A is better. Table 1 shows the average RMSE and R^2 of six subjects using Feature A (F.A) and Feature (F.B). It can be seen from Table 1 that R^2 of Feature A is higher than Feature B which indicates that Feature A has a better performance.

Table 1: The average estimation performance index.

	Subject A		Subject B		Subject C		Subject D		Subject E		Subject F	
	F.A	F.B	F.A	F.B	F.A	F.B	F.A	F.B	F.A	F.B	F.A	F.B
RMSE	3.24	4.23	2.95	5.35	3.57	3.92	3.06	3.20	3.96	3.98	4.05	3.98
R^2	0.81	0.78	0.81	0.79	0.83	0.77	0.87	0.80	0.82	0.79	0.83	0.81

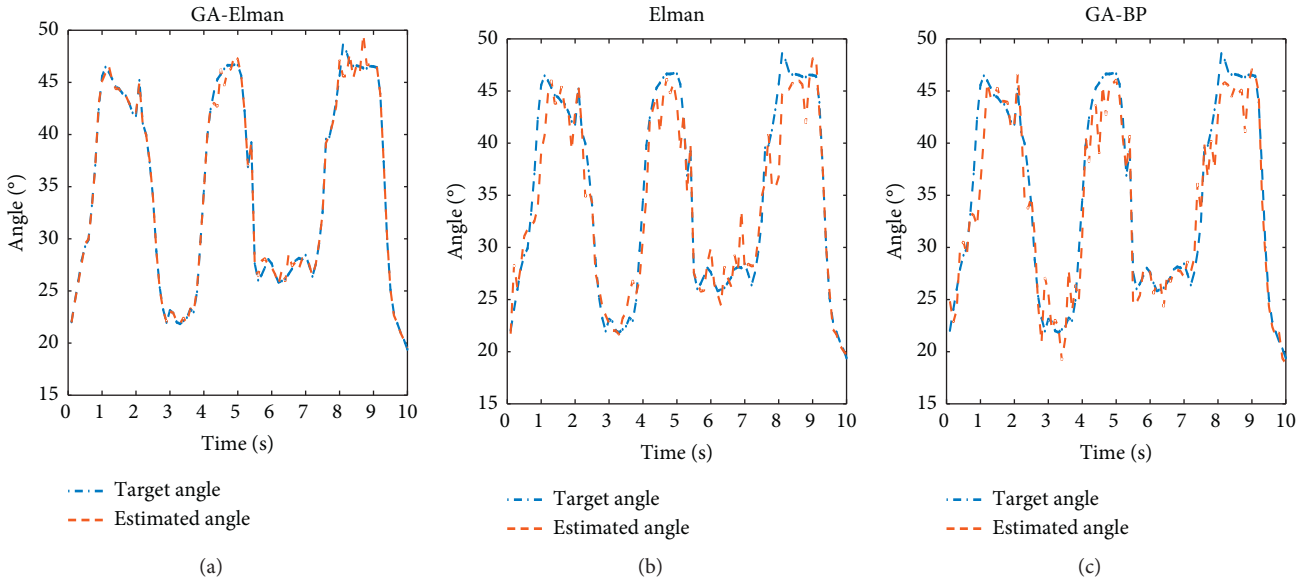

Figure 8: Estimated result using different NN. (a) GA-Elman NN. (b) Elman NN. (c) GA-BP NN.

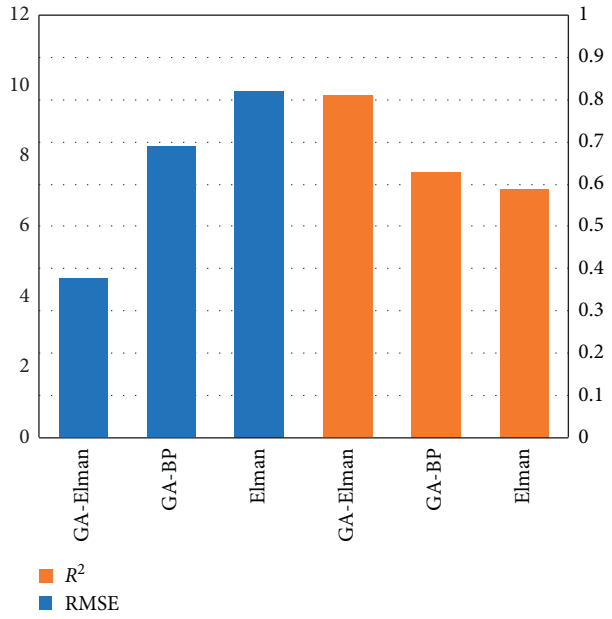

Figure 9: The RMSE and R^2.

Taking one subject as an example, Figure 8 is the comparison of the actual shoulder joint angles and the estimated shoulder joint angles by using Feature A with GA-Elman, Elman, and GA-BP, respectively. Figure 9 shows the average RMSE and R^2 of different neural networks.

It can be seen from Figure 8 that prediction results of GA-Elman are the best. It can be seen from Figure 9 that GA-Elman has the lowest RMSE and highest R^2. Comparing the three neural network prediction results shows that GA-Elman performance is best. By analysing the

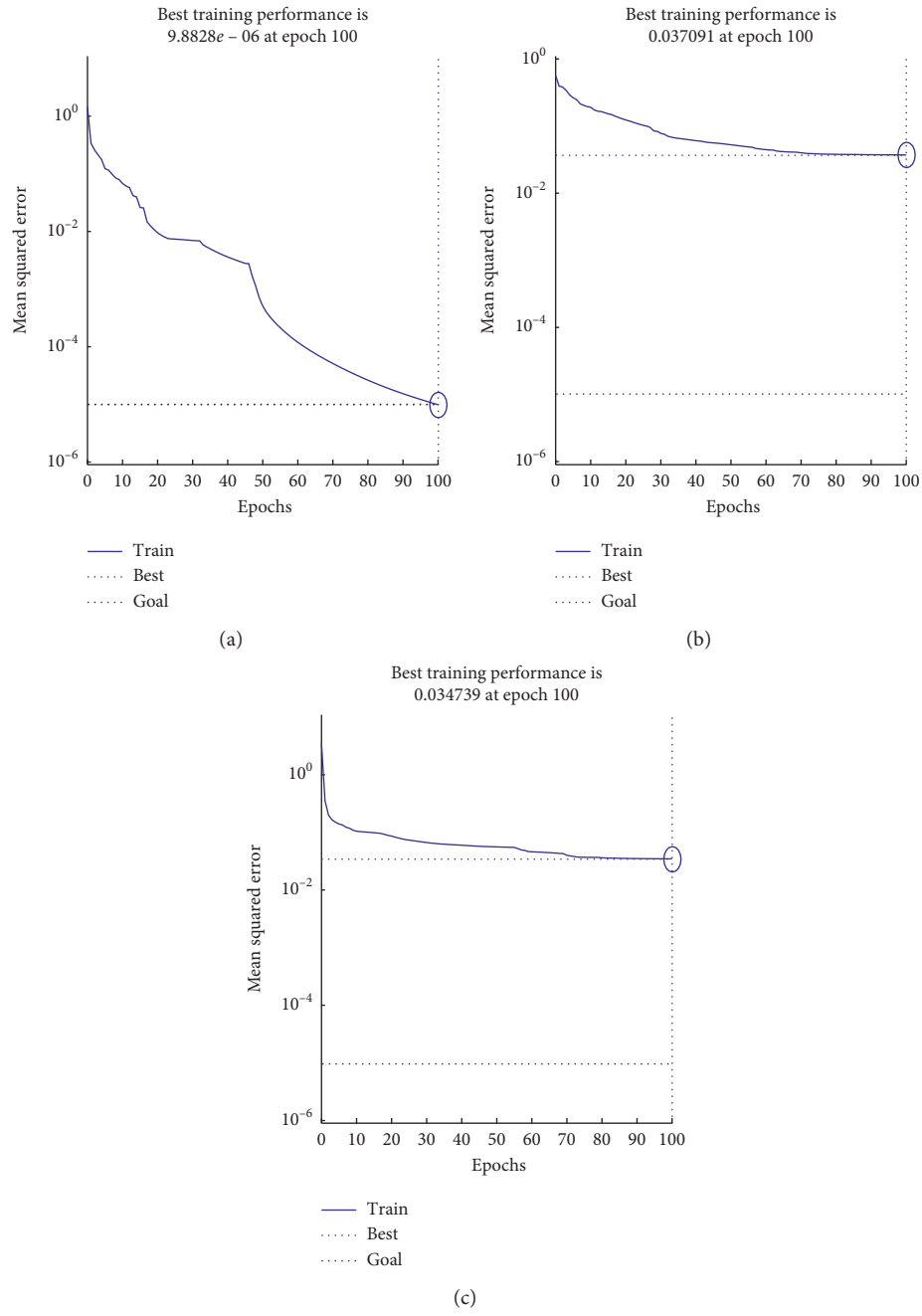

Figure 10: Network training error curve. (a) GA-Elman NN. (b) Elman NN. (c) GA-BP NN.

error curve and fitness curve in the prediction process, GA-Elman showed the best performance. Figure 10 shows the network training error curves for different neural networks. Figure 11 is the fitness curve for two neural networks.

The error continuously decreases until the target network training error is reached during the training process. Figures 10(b) and 10(c) show that the Elman NN error has a downward trend. However, the smallest errors are still higher than the error of GA-Elman.

As can be seen from Figure 11 with the increase of evolutionary algebra, the fitness of GA-Elman and GA-BP has decreased. The fitness of GA-Elman decreased rapidly during the 0–5 evolution. The fitness afterward did not change much. This shows that the error of GA-Elman is smaller during the evolution process. The estimated results are also more accurate.

The above conclusions show that GA-Elman is superior in both the prediction process and the prediction results. Figures 12 and 13 show the average RMSE and the average R^2 for every subject.

It is shown in Figures 12 and 13 that GA-Elman exhibits excellent estimation performance in each experiment of subjects. The average RMSE of the B subject reaches the lowest, which was 2.95. The average R^2 of the D subject reaches the highest, which was 0.87.

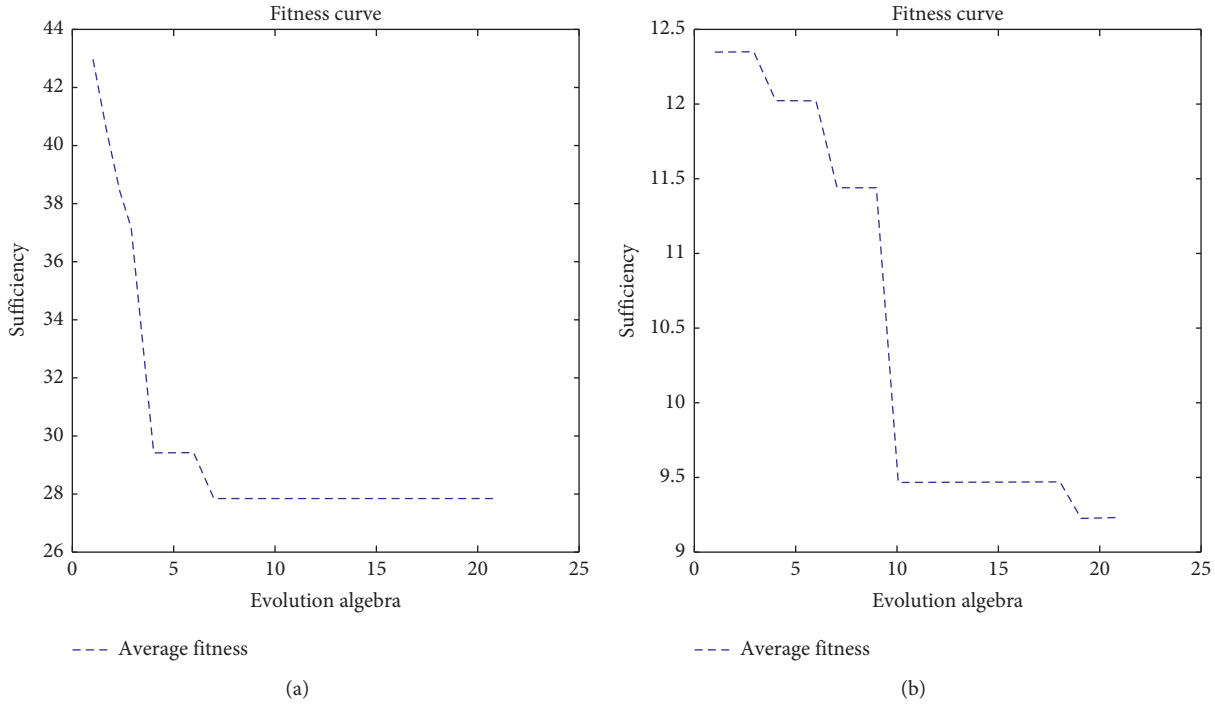

Figure 11: Fitness curve. (a) GA-Elman NN. (b) GA-BP NN.

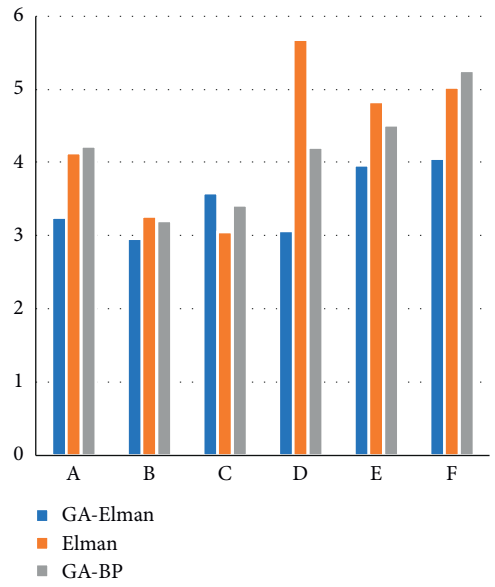

Figure 12: The average RMSE.

3.2. Estimation of Shoulder and Elbow Joints. The GA-Elman with Feature A estimates the continuous angle of the shoulder and elbow joints simultaneously and compares with the GA-BP and Elman neural networks. Table 2 shows the estimated RMSE and R^2.

As can be seen from Table 2, the GA-Elman has the lowest RMSE and the highest R^2, which shows that the prediction model also has the best performance for simultaneous continuous estimation. The estimated performance trends for the three models are consistent for the same subjects which indicate that the model does not differ from the individual. Compared with Table 1, Synchronous estimation is less effective than single joint estimation. But synchronization estimates are not bad. The highest R^2 is 0.7723 and RMSE is 7.1421 in synchronous estimation by using GA-Elman with Feature A.

So far, the reliability of the joint continuous motion estimation framework based on SEMG signals has been proved. The framework we introduced shows three comparative advantages. First, the selection of a specific subspace

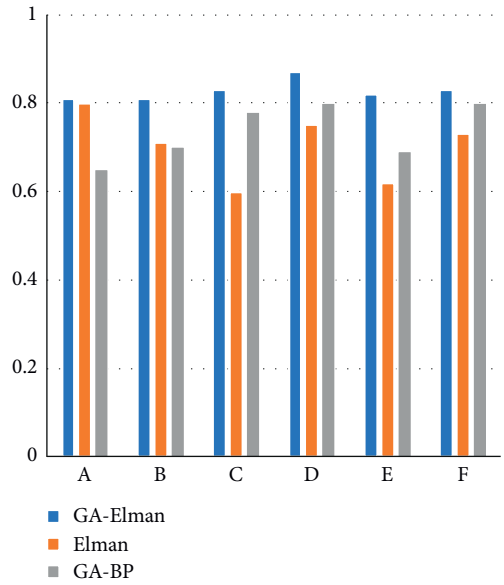

Figure 13: The average R^2.

Table 2: RMSE and R^2 estimated by subjects using three NNs.

			GA-Elman	GA-BP	Elman
Subject A	Shoulder	RMSE	4.1417	7.3099	10.2045
		R^2	0.7833	0.5918	0.4514
	Elbow	RMSE	5.1253	8.3085	9.3042
		R^2	0.8222	0.5041	0.6763
Subject B	Shoulder	RMSE	3.0728	6.3099	10.1078
		R^2	0.8142	0.7015	0.5912
	Elbow	RMSE	7.1421	4.8686	8.5155
		R^2	0.7723	0.8203	0.6565
Subject C	Shoulder	RMSE	6.1708	10.1952	8.1873
		R^2	0.7841	0.5480	0.6521
	Elbow	RMSE	1.1358	7.2054	9.2116
		R^2	0.8556	0.7489	0.4302
Subject D	Shoulder	RMSE	3.1324	6.1982	6.1745
		R^2	0.8764	0.6102	0.6975
	Elbow	RMSE	3.0988	10.2543	10.1865
		R^2	0.7874	0.4972	0.6153
Subject E	Shoulder	RMSE	4.1053	9.2633	9.1954
		R^2	0.7954	0.6645	0.6253
	Elbow	RMSE	5.1623	8.2845	10.2064
		R^2	0.8133	0.6572	0.5382
Subject F	Shoulder	RMSE	3.2588	8.0483	8.4527
		R^2	0.8253	0.7235	0.6348
	Elbow	RMSE	4.3527	7.6523	7.2594
		R^2	0.8075	0.7838	0.6972

in wavelet packet transform not only extracts signals that match the motion, but also achieves dimensionality reduction, which greatly reduces the number of features. Redundant sEMG signals make it difficult to predict movement. The introduction of wavelet packet energy entropy in non-adjacent spaces can alleviate this problem. Compared with the original wavelet packet energy entropy, this method is more accurate in motion estimation. But it did not increase the difficulty of calculation. Secondly, GA-Elman was established to deal with the regression problem of continuous motion. Finally, the feasibility of estimating single joint and multijoint movements was verified in a large number of upper limb movements. Compared with Elman and GA-BP NN, the average RMSE of GA-Elman is reduced by about 25% and the average R^2 is increased by about 30% in single joint motion estimation. In multijoint motion estimation, it shows similar performance. However, the volunteers in the experiment are all healthy. Later, patients with dyskinesia can be considered for the experiment. The addition of genetic algorithm has also slowed down the prediction efficiency to a certain extent.

4. Conclusions

In this paper, aiming at the rehabilitation training of patients with hemiplegia, the Elman neural network optimized by GA is proposed to predict the shoulder and elbow joint angle. The WPEE of the specific subspace is used to represent the sEMG as the input of the neural network. The results show that the method in this paper is effective for estimating the shoulder and elbow joint angle of the upper limb. In comparative experiments, it showed the best performance. However, the comparison of Tables 1 and 2 shows that the predictive performance of synchronous continuous motion is lower than that of single joint motion because of the effect of muscle synergy. In future work, to better improve the estimation performance, the impact of muscle synergy will be considered during synchronous exercise.

Data Availability

The data used to support the findings of this study are available from the corresponding author upon request.

Conflicts of Interest

The authors declare that they have no conflicts of interest.

Acknowledgments

This work was supported by the National Natural Science Foundation of China (Nos. 61971169 and U1909209), National Natural Science Major Foundation of Research Instrumentation of China (Grant no. 61427808), and Zhejiang Provincial Natural Science Foundation of China (Grant no. LZ17F030002).

References

[1] K. Monte-Silva, D. Piscitelli, N. Norouzi-Gheidari, M. A. P. Batalla, P. Archambault, and M. F. Levin, "Electromyogram-related neuromuscular electrical stimulation for restoring wrist and hand movement in Poststroke hemiplegia: a systematic review and meta-analysis," *Neurorehabilitation and Neural Repair*, vol. 33, no. 2, pp. 96–111, 2019.

[2] H. Tsao, K. Pannek, R. N. Boyd, and S. E. Rose, "Changes in the integrity of thalamocortical connections are associated with sensorimotor deficits in children with congenital hemiplegia," *Brain Structure and Function*, vol. 220, no. 1, pp. 307–318, 2015.

[3] M. S. Kim, S. H. Kim, S. E. Noh, and K. M. Lee, "Robotic-assisted shoulder rehabilitation therapy effectively improved poststroke hemiplegic shoulder pain: a randomized controlled trial," *Archives of Physical Medicine and Rehabilitation*, vol. 100, no. 6, pp. 1015–1022, 2019.

[4] M. Hassan, H. Kadone, T. Ueno, Y. Hada, Y. Sankai, and K. Suzuki, "Feasibility of synergy-based exoskeleton robot control in hemiplegia," *IEEE Transactions on Neural Systems and Rehabilitation Engineering*, vol. 26, no. 6, pp. 1233–1242, 2018.

[5] F. Vanoglio, P. Bernocchi, C. Mulè et al., "Feasibility and efficacy of a robotic device for hand rehabilitation in hemiplegic stroke patients: a randomized pilot controlled study," *Clinical Rehabilitation*, vol. 31, no. 3, pp. 351–360, 2017.

[6] Y. Li, X. Zhang, Y. Gong, Y. Cheng, X. Gao, and X. Chen, "Motor function evaluation of hemiplegic upper-extremities using data fusion from wearable inertial and surface EMG sensors," *Sensors*, vol. 17, no. 3, p. 582, 2017.

[7] X. F. Zhang, X. Li, J. T. Dai et al., "The design of a hemiplegic upper limb rehabilitation training system based on surface EMG signals," *Journal of Advanced Mechanical Design, Systems, and Manufacturing*, vol. 12, no. 1, Article ID JAMDSM0031, 2018.

[8] N. Balendra and J. E. Langenderfer, "Effect of hammer mass on upper extremity joint moments," *Applied Ergonomics*, vol. 60, pp. 231–239, 2017.

[9] M. D. Ellis, I. Schut, and J. P. A. Dewald, "Flexion synergy overshadows flexor spasticity during reaching in chronic moderate to severe hemiparetic stroke," *Clinical Neurophysiology*, vol. 128, no. 7, pp. 1308–1314, 2017.

[10] K. Wang, X. Zhang, J. Ota, and Y. Huang, "Estimation of handgrip force from SEMG based on wavelet scale selection," *Sensors*, vol. 18, no. 2, p. 663, 2018.

[11] Z. G. Xiao and C. Menon, "Performance of forearm FMG and sEMG for estimating elbow, forearm and wrist positions," *Journal of Bionic Engineering*, vol. 14, no. 2, pp. 284–295, 2017.

[12] L. Pan, D. Zhang, J. Liu, X. Sheng, and X. Zhu, "Continuous estimation of finger joint angles under different static wrist motions from surface EMG signals," *Biomedical Signal Processing and Control*, vol. 14, pp. 265–271, 2014.

[13] J. Han, Q. Ding, A. Xiong, and X. Zhao, "A state-space EMG model for the estimation of continuous joint movements," *IEEE Transactions on Industrial Electronics*, vol. 62, no. 7, pp. 4267–4275, 2015.

[14] Q. Zhang, R. Liu, W. Chen, and C. Xiong, "Simultaneous and continuous estimation of shoulder and elbow kinematics from surface EMG signals," *Frontiers in Neuroscience*, vol. 11, p. 80, 2017.

[15] G. Huang, Z. Xian, Z. Zhang, S. Li, and X. Zhu, "Divide-and-conquer muscle synergies: a new feature space decomposition approach for simultaneous multifunction myoelectric control," *Biomedical Signal Processing and Control*, vol. 44, pp. 209–220, 2018.

[16] F. Xiao, Y. Wang, Y. Gao, Y. Zhu, and J. Zhao, "Continuous estimation of joint angle from electromyography using multiple time-delayed features and random forests," *Biomedical Signal Processing and Control*, vol. 39, pp. 303–311, 2018.

[17] Q. Ding, J. Han, and X. Zhao, "Continuous estimation of human multi-joint angles from sEMG using a state-space model," *IEEE Transactions on Neural Systems and Rehabilitation Engineering*, vol. 25, no. 9, pp. 1518–1528, 2017.

[18] J. Liu, S. H. Kang, D. L. Xu, Y. P. Ren, S. J. Lee, and L. Q. Zhang, "EMG-based continuous and simultaneous estimation of arm kinematics in able-bodied individuals and stroke survivors," *Frontiers in Neuroscience*, vol. 11, p. 480, 2017.

[19] S. Pancholi and A. M. Joshi, "Improved classification scheme using fused wavelet packet transform based features for intelligent myoelectric prostheses," *IEEE Transactions on Industrial Electronics*, 2019, In press.

[20] C. Sravani, V. Bajaj, S. Taran, and A. Sengur, "Flexible analytic wavelet transform based features for physical action identification using sEMG signals," *IRBM*, vol. 41, no. 1, pp. 18–22, 2019.

[21] K. Z. Takahashi, M. D. Lewe, and G. S. Sawicki, "A neuromechanics-based powered ankle exoskeleton to assist walking post-stroke: a feasibility study," *Journal of NeuroEngineering and Rehabilitation*, vol. 12, no. 1, pp. 12–23, 2015.

[22] Y. Zhang, B. Liu, X. Ji, and D. Huang, "Classification of EEG signals based on autoregressive model and wavelet packet decomposition," *Neural Processing Letters*, vol. 45, no. 2, pp. 365–378, 2016.

[23] K. Huang and S. Aviyente, "Information-theoretic wavelet packet subband selection for texture classification," *Signal Processing*, vol. 86, no. 7, pp. 1410–1420, 2006.

[24] K. Krzysztof, S. Aleksandra, K. Rafał, P. Janusz, and R. Andrzej, "Multisensor data fusion using Elman neural networks," *Applied Mathematics and Computation*, vol. 319, pp. 236–224, 2018.

[25] P. I. Earnest and M. C. Krishna, "Human action recognition using genetic algorithms and convolutional neural networks," *Pattern Recognition*, vol. 59, pp. 199–212, 2016.

[26] W. Teekeng and A. Thammano, "Modified genetic algorithm for flexible job-shop scheduling problems," *Procedia Computer Science*, vol. 12, pp. 122–128, 2012.

[27] K. J. Wei, D. Zhao, Y. J. Zheng, and S. J. Hou, "A novel optimized GA–Elman neural network algorithm," *Neural Computing and Applications*, vol. 31, no. 2, pp. 449–459, 2019.